國立清華大學電機工程學系

實作專題報告

題　　目:

無橋升壓切換式整流器之研製及其散熱扇驅動應用

Development of Bridgeless Boost Switch-Mode Rectifier and Its Cooling Fan Driving Application

組　別：A105

組　員：許明澤 (學號 105061136)

haha36376@gmail.com

指導老師：廖聰明 教授

中華民國 109 年 11 月 22 日

Abstract

This special topic develops a bridgeless boost switch-mode rectifier (SMR) fed switched-reluctance motor (SRM) driven cooling fan. First, the single-phase boost SMR front-end is designed and implemented. Thanks to the bridgeless schematic, it possesses higher efficiency compared with the standard SMR. The power circuit and control scheme are all properly designed. The multiplier based current control scheme and voltage controller are realized using operational amplifier based analog circuits.

Next, the SRM-driven fan is established. Its asymmetric bridge converter is constructed using off-the-shelf SRM insulated-gate bipolar transistor (IGBT) intelligent power module (IPM). The commutation and pulse width modulated (PWM) switching controls are conducted according to the sensed Hall position signals. And the speed control scheme with direct duty ratio regulation is applied.

Finally, the experimental performance evaluation for the whole SMR-fed SRM-driven fan is made. In addition, the experimental comparative evaluation of the cooling fan powered by the diode rectifier, the standard boost SMR and the bridgeless boost SMR is also made.

Keywords: Boost SMR, bridgeless, PFC, SRM, cooling fan, control, analog circuit.

摘 要

本專題旨在建構一以無橋式升壓切換式整流器供電之開關式磁阻馬達驅動冷卻風扇。首先，設計及實現一單相升壓切換式整流器前級。由於無橋式之架構，其相較於標準型切換式整流器具有較高之效率。電力電路及控制機構均妥善設計。而基於乘法器之電流控制架構及電壓控制器，藉運算放大器為主之類比電路得以實現。

接著，建構開關式磁阻馬達驅動之散熱風扇，其非對稱橋式轉換器，以市售切換式磁阻馬達專用絕緣閘雙極電晶體智慧型功率模組組立之。根據感測之霍爾位置訊號，從事換相及脈波寬度調變控制。而風扇之速度控制，採直接責任週期比調節方式。

最後，以一些實測結果，驗證所建切換式整流器供電開關式磁阻馬達驅動冷卻風扇之整體操控性能。另外亦從事以不同交流前級供電冷卻風扇之比較性能實測評定，包含二極體整流器、標準型升壓切換式整流器、以及所建之無橋式升壓切換式整流器。

關鍵詞: 升壓切換式整流器、無橋式、功率因數矯正、切換式磁阻馬達、散熱風扇、控制、類比電路。

I. INTRODUCTION

For a motor driven cooling fan, its input power is proportional to the cubic of speed ($P = T_L \omega_r \propto \omega_r^3$) [1]. Hence, a converter-fed variable speed motor driven fan can achieve great energy saving. Till now, single-phase induction motor and brushless DC motor (BDCM) are still the most commonly used ones in this application. However, SRM also has the potential as an alternative owing to tis many merits.

SRM [2] belongs to the electric machine with doubly-salient and singly-excited with concentrated windings. It is rigid and suitable for high-speed operation. Moreover, the rotor of SRM is not equipped with conductors or permanent magnets, this makes it have no cogging torque and easy to start. In driving operation, its converter circuit is simple with fault-tolerant capability. The high generating torque and acceleration capabilities make it possess high application potential [3-7]. Among the existing SRM converters [8-13], the asymmetric bridge converter has the largest PWM switching flexibility. Hence it is adopted for the developed SRM-driven fan. In driving control, the commutation instant setting and voltage boosting are the most critical effecting factors for SRM driving performance. In the developed cooling fan, the DC-link voltage of SRM drive is powered by a boost SMR from the mains to have well-regulated and boostable DC-link voltage. Moreover, the commutation and switching schemes are properly designed to preserve satisfactory operating characteristics. In speed control, for the ease of realization using analog circuits, the direct duty-ratio mode for the speed controller is adopted.

For a motor drive powered by the mains, one can use the proper type of SMR to establish the boosted and well-regulated DC-link voltage. The improved driving characteristics with good line drawn power quality can be obtained simultaneously. The surveys for the single-phase SMRs can be found in [14-19]. Among various SMRs, the boost SMR possesses the best PFC control performance. By adopting the bridgeless schematic [20-22], the efficiency can be increased due to the less diode voltage drops. Hence, it is adopted for the established motor driven cooling fan.

The design and implementation of a single-phase boost SMR-fed SRM-driven cooling fan are presented in this report. The employed SRM is rated as three-phase 6/4, 70W, 900rpm. The asymmetric bridge converter is constructed using two off-the-shelf two-phase SRM IGBT IPMs FCAS30DN60BB by the Fairchild Semiconductor. For simplicity, the direct duty-ratio controls for both the PWM switching scheme and the open speed loop are adopted for the established SRM-driven fan. To let the developed fan be powered from the mains with good line drawn power quality, a single-phase bridgeless boost SMR front-end is established. Some measured results are provided to evaluate the operation performance of the established SMR-fed cooling fan. Both standard and bridgeless boost SMRs are comparatively assessed.

II. INTRODUCTORY OF SWITCHED-RELUCTANCE MOTOR AND SWITCH-MODE RECTIFIER

2.1 Switched-reluctance Motors

A. Structural Features

Fig. 2.1(a) shows the configuration of a 3-phase 6/4 SRM. It possesses the doubly-salient and singly-excited structure. The concentrated phase armature winding excitation with quasi square-wave current is made according to the sensed rotor absolute position. Since SRM is dedicated for speed driving applications, it tends to have smaller numbers of stator and rotor teeth. The most commonly used SRMs include 3-phase 6/4, 3-phase 12/8, 3-phase 12/10 and 4-phase 8/6. Fig. 2.1(b) depicts the photo of the employed three-phase 6/4 SRM. And the measured winding inductance profile at $f = 100\text{Hz}$ is plotted in Fig. 2.1(c).

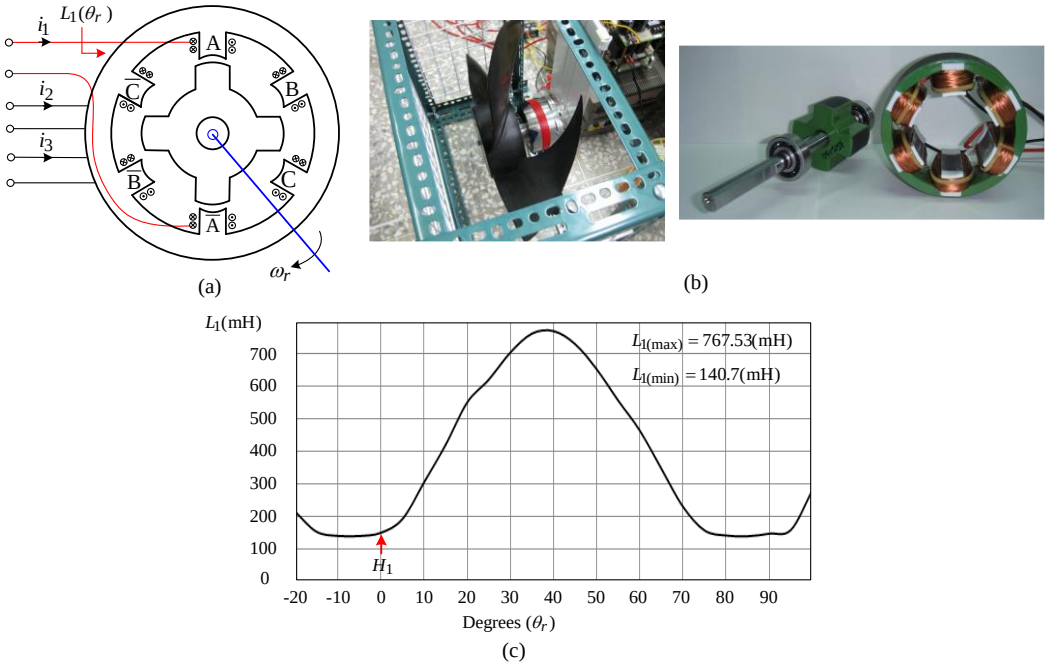

Fig. 2.1. Configuration and the employed SRM: (a) a three-phase 6/4 SRM; (b) photo of the employed three-phase 6/4 SRM; (c) measured winding inductance profile.

B. Governing Equations

By assuming linear magnetic circuit and neglecting inter-phase coupling effects the phase winding voltage equation of an SRM can be expressed as:

$$v = Ri + \frac{d\lambda(i,\theta_r)}{dt} = Ri + L(i,\theta_r)\frac{di}{dt} + \frac{\partial L(i,\theta_r)}{\partial \theta_r}\omega_r i \triangleq Ri + L(i,\theta_r)\frac{di}{dt} + e(i,\omega_r,\theta_r) \tag{2.1}$$

where v = winding terminal voltage, i = winding current, R = winding resistance, $L(i,\theta_r)$ = winding inductance, $e(i,\omega_r,\theta_r)$ = back-electromagnetic force (EMF), θ_r = rotor angular position, ω_r = rotor angular speed. (2.1) indicates that: (i) the back-EMF of an SRM depends on rotor speed and winding current; (ii) the winding current tracking waveform is affected by the back-EMF and the winding inductance.

The measured winding inductance profile of the employed SRM at different rotor positions using the LCR-meter (Hioki IM 3536) under 100Hz indicates the maximum and minimum winding inductances are $L_{A(\max)} = 767.35\,(\text{mH})$ and $L_{A(\min)} = 140.7\,(\text{mH})$. The phase average winding resistance is $R_s = 30.7\,\Omega$.

The per-phase electromagnetic developed torque T_{ei} and thus the composite torque T_e of an SRM can be derived from its energy as:

$$T_e = \sum_{i=1}^{N} T_{ei} = \sum_{i=1}^{N} \frac{1}{2} i_i^2 \frac{\partial L(i_i,\theta_r)}{\partial \theta_r} \triangleq \sum_{i=1}^{N} k_{ti}(i_i^2) = T_L + B\omega_r + J\frac{d\omega_r}{dt} \tag{2.2}$$

where $k_{ti} \triangleq 0.5\partial L(i_i,\theta_r)/\partial\theta_r$, N = phase number, T_L = load torque, J = total moment of inertia, B = total damping ratio. It is obvious from (2.2) that the torque generating characteristic of an SRM is similar to the series DC motor ($T_{ei} \propto i_i^2$). Thus, it possesses high starting torque and acceleration ability.

C. SRM Converters

Till now, a lot of SRM converters have been developed. Fig. 2.2(a) shows the most commonly used asymmetric bridge converter with 2N (N = phase number) switches and

diodes. Every phase winding can be magnetized and de-magnetized independently. The schematics and current paths of phase-1 winding in three modes are illustrated in Figs. 2.2(b) to 2.2(d). Mode 1 and mode 2 are employed in performing normal PWM current control in motoring mode. However, mode 1 and mode 3 must be used to counter the effects of negative back-EMF in an SRG. The asymmetric bridge converter is adopted in the developed SRM drive.

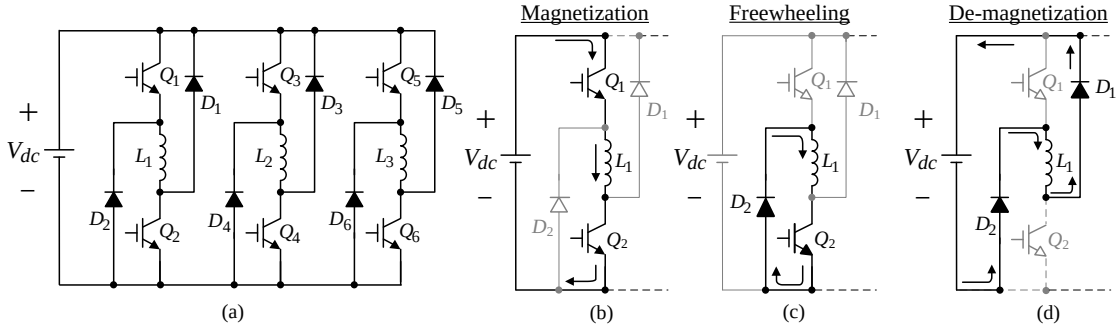

Fig. 2.2. Asymmetric bridge converter and winding current paths: (a) circuit; (b) mode 1: magnetization; (c) mode 2: freewheeling; (d) mode 3: de-magnetization.

2.2 Switch-mode Rectifiers

For a motor drive powered from the mains, switch-mode rectifier (SMR) can be employed as an active AC front-end to establish boostable and well-regulated DC-link voltage, meanwhile to meet the AC line drawn power quality requirements. Till now, there were a lot of existing single-phase SMRs, each type possesses its features and suitable application occasions.

Seven types of single-phase boost SMRs as shown in Figs. 2.3(a) to 2.3(g) have been comparatively evaluated. Wherein SMR-S is the most commonly used standard boost SMR. Recently, the bridgeless boost SMR shown in Fig. 2.3(h) has also been proposed to enhance the efficiency. In this report, both the standard and the bridgeless boost SMRs are developed and comparatively evaluated.

2.2.1 Standard Boost SMR

The power circuit and control scheme of a standard SMR in CCM are shown in Fig. 2.4. This control system belongs to multi-loop configuration consisting of inner RC-CCPWM scheme and outer voltage loop. In the inner current loop, its command is generated by multiplying the magnitude yielded from the voltage loop with a unit-vector synchronized with the AC input voltage.

2.2.2. Bridgeless Boost SMR

The power circuit and control scheme of the developed bridgeless boost SMR are shown in Fig. 2.5. The diode bridge rectifier is removed, and two switches with anti-paralleled diodes are equipped. The two switches in Fig. 2.5 are simultaneously operated. Comparing Fig. 2.5 to Fig. 2.4 one can find that one diode voltage drop is reduced during both PWM ON and OFF intervals for the bridgeless SMR. During positive half voltage cycle ($v_{ac} > 0$) the current paths of this bridgeless SMR at PWM ON and OFF intervals are shown in Figs. 2.6(a) and 2.6(b). From the equivalent circuits, one can find that the switching operations of the bridgeless SMR are the same as the standard boost SMR shown in Fig. 2.4.

Although the efficiency of bridgeless SMR can be slightly increased, it possesses the common mode EMI problem due to the large parasitic capacitance between the output and ground, which provides a relatively low impedance path. To reduce this problem, the boosting inductor is divided into two equal inductors, and they are placed at the input AC source side.

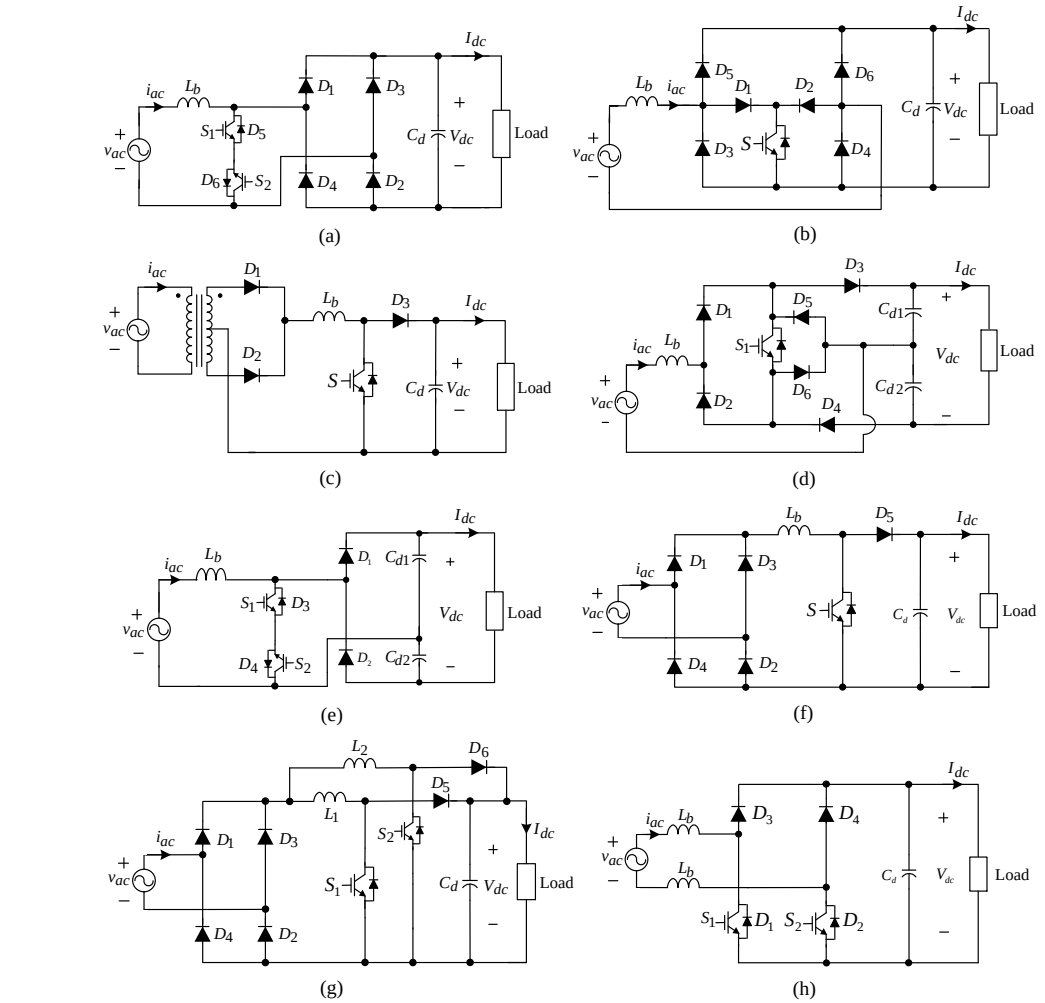

Fig. 2.3. Eight single-phase non-isolated boost SMR circuits: (a) SMR-A; (b) SMR-B; (c) SMR-C; (d) SMR-D; (e) SMR-E; (f) SMR-S; (g) M-SMR; (h) bridgeless SMR.

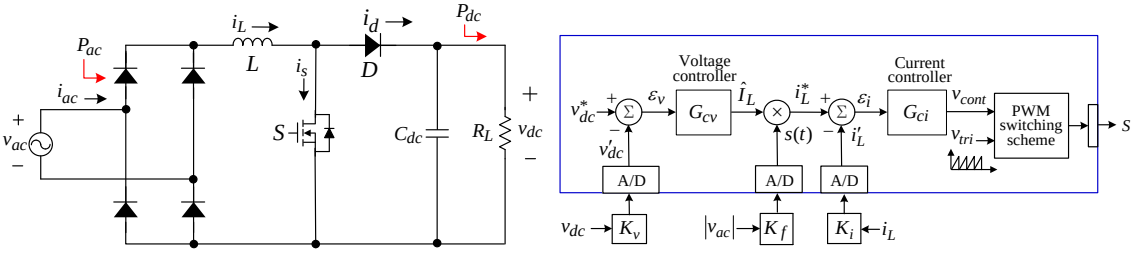

Fig. 2.4. Schematic and control scheme of the developed standard boost SMR.

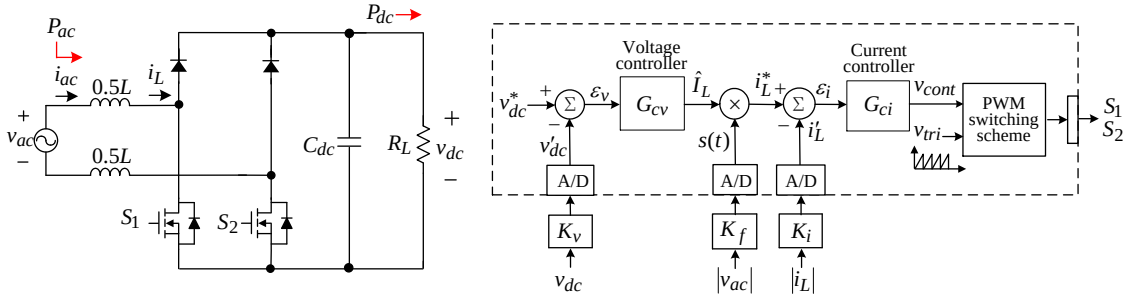

Fig. 2.5. Schematic and control scheme of the developed bridgeless boost SMR.

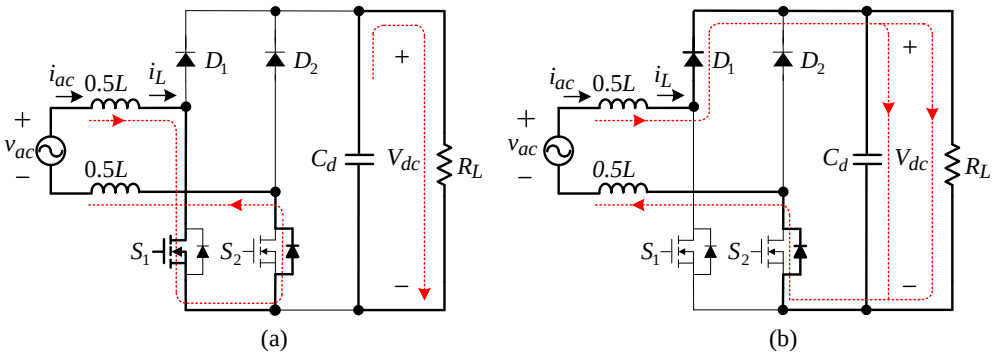

Fig. 2.6. Circuit operations during positive half voltage cycle: (a) PWM ON magnetization mode; (b) PWM OFF demagnetization mode.

III. THE ESTABLISHED SMR-FED SRM DRIVEN FANS

3.1. SRM-driven Fan

Fig. 3.1(a) shows the schematic of the SRM-driven cooling fan. The open speed loop with direct duty ratio control is adopted for the developed SRM-driven fan. Fig. 3.1(a) also shows the system block diagram of the commutation signal and PWM switching signal generation scheme. The commutation and PWM switching controls are made according to the sensed Hall position signals. The analog realization circuit is shown in Fig. 3.1(b).

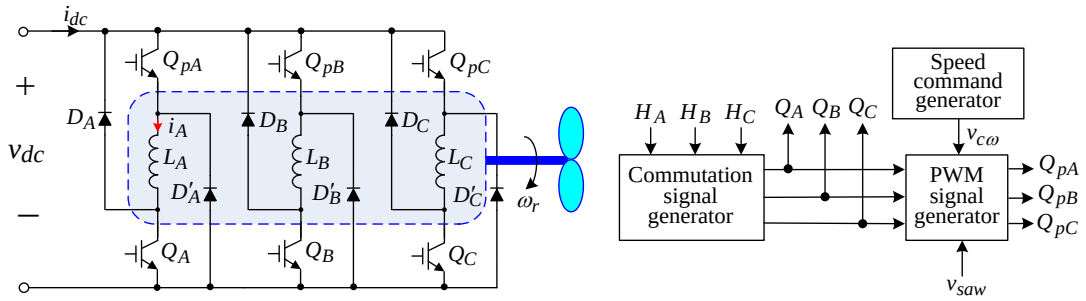

(a)

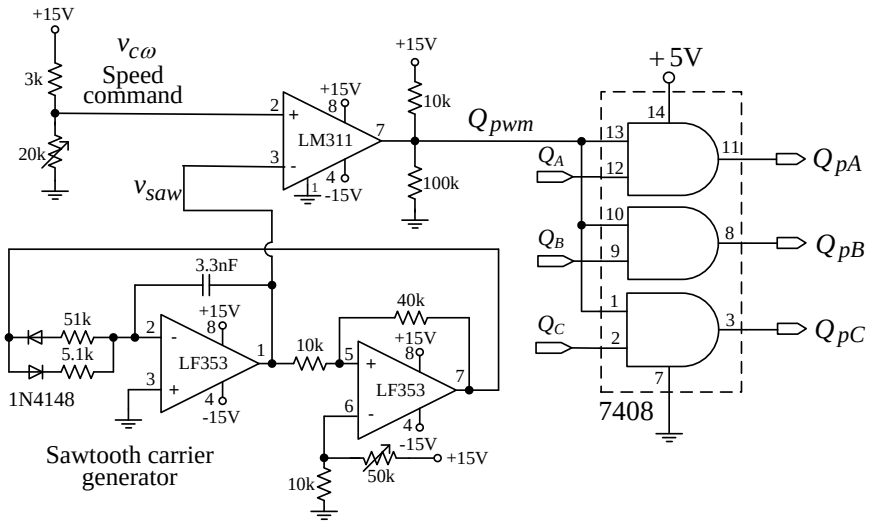

(b)

Fig. 3.1. SRM-driven cooling fan: (a) schematic and PWM signal generating scheme; (b) PWM switching signal generation circuit.

3.2. Diode Rectifier Powered SRM Driven Cooling Fan

Fig. 3.2(a) shows the schematic of the established diode rectifier-fed SRM-driven fan. The measured (v_{ac}, i_{ac}) with input $V_{ac} = 110\text{V}/60\text{Hz}$ at the speeds of 500rpm and 700rpm are plotted in Figs. 3.2(b) and 3.2(c). And the corresponding steady-state characteristics are listed in Table 3.1. As observed from the measured results, the peaky line drawn currents with bad power quality characteristics are yielded.

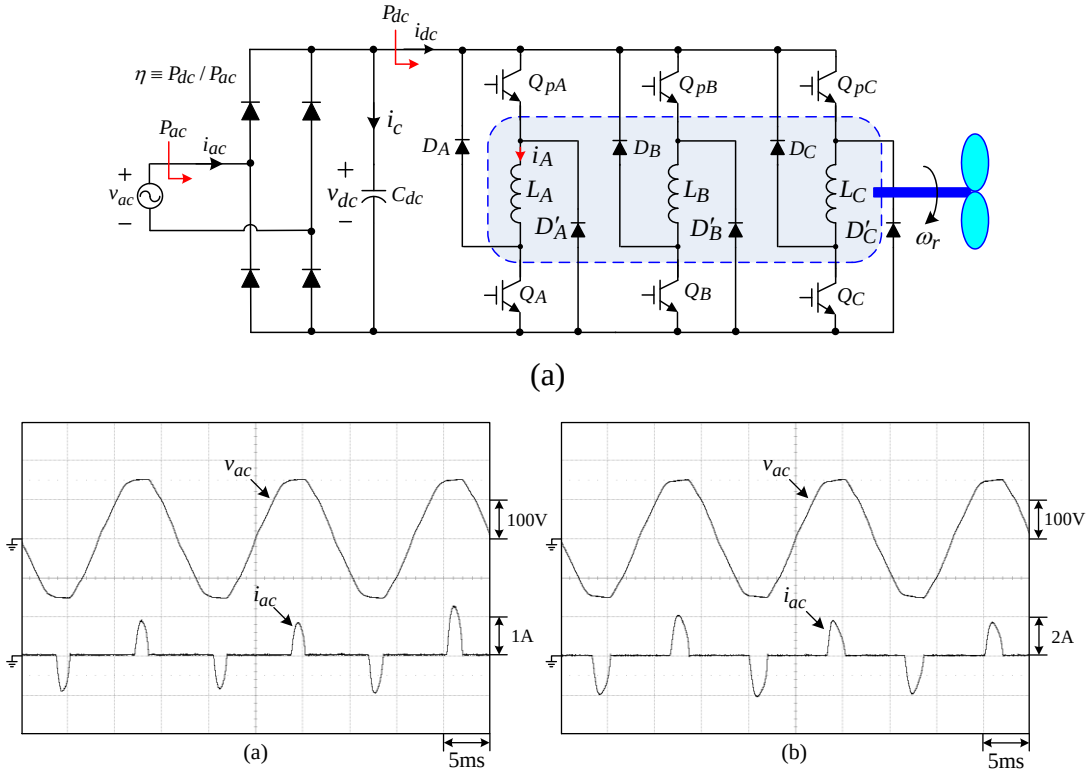

Fig. 3.2. Diode rectifier-fed SRM-driven cooling fan: (a) schematic; (b) measured (v_{ac}, i_{ac}) under $(V_{ac} = 110\text{V}/60\text{Hz})$ at 500rpm; (c) measured (v_{ac}, i_{ac}) under $(V_{ac} = 110\text{V}/60\text{Hz})$ at 700rpm.

Table 3.1: Measured steady-state characteristics of the established diode rectifier-fed SRM-driven cooling fan under various speeds

Speed (rpm)	300	400	500	600	700
V_{ac} (V)	109.62	109.55	109.3	108.95	109.5
I_{ac} (A)	0.1144	0.1914	0.3077	0.4333	0.6900
P_{ac} (W)	6.06	10.48	18.08	27.52	45.88
V_{dc} (V)	149.01	148.73	147.72	145.77	147.16
I_{dc} (A)	0.038	0.066	0.115	0.183	0.303
P_{dc} (W)	5.62	9.77	16.94	26.71	44.64
PF	0.4832	0.4999	0.5376	0.583	0.6073
$\eta \triangleq (P_{dc} / P_{ac})$	92.68%	93.19%	93.69%	97.05%	97.29%
THD_i	174.87%	163.24%	151.77%	133.97%	127.89%

3.3. Bridgeless Boost Switch-mode Rectifier

A. Power Circuit

The power circuit of the developed bridgeless boost SMR is shown in Fig. 3.3(a). The system variables are listed below:

- AC input: $V_{ac} = 110\text{V}/60\text{Hz}$.
- DC output: $V_{dc} = 200\,\text{V}$.
- Switching frequency: $f_s = 20\text{kHz}$.
- Energy storage inductors and filtering capacitor: $L_1 = L_2 = 3.5\text{mH}, C_{dc} = 1000\mu\text{F}$.
- Power switches S_a, S_b: W20NK50Z

B. Control Scheme

The control scheme of the developed bridgeless boost SMR is shown in Fig. 3.3(b). The outer voltage loop adopts PI feedback control. As to the inner current loop, the PI feedback controller is augmented with a robust tracking error cancellation controller with a weighting function $W_i(s)$. The analog realization circuit is shown in Fig. 3.3(c). The voltage sensing factor and the feedback controllers $G_{cv}(s), G_{ci}(s)$ and $W_i(s)$ are set as:

$$K_v = 0.0025\text{V/V},\ \ K_f = 0.0909\text{V/V},\ \ K_i = 1.6\text{V/A} \tag{1}$$

$$G_{cv}(s) = 2.45 + \frac{19.6}{s},\ \ G_{ci}(s) = 11.76 + \frac{19.6}{s},\ \ W_i(s) = \frac{0.5}{1 + 0.0001s} \tag{2}$$

C. Measured Results

(a) Unit-sine function

As indicated in Fig. 3.3(b), the unit-sine being synchronized with v_{ac} is needed for realizing the inner current control loop of the boost SMR. Fig. 3.4 shows the measured grid voltage v_{ac}, sensed voltage v'_{ac} and the resulted unit-sine function $|v'_{ac}|$. The results indicate the successful generation of in-phase unit-sine function.

(b) Steady-state characteristics

In the following measured results, the resistive load is connected to the DC-link of the bridgeless boost SMR for preliminary test. Figs. 3.5 and 3.6 show the measured results by PI control under two resistive loads. The well-regulated DC-link voltage can be seen, but the zero-crossing distortion of currents by PI control exists. The current robust tracking error cancellation controller may improve this problem. Figs. 3.7 and 3.8 show the measured results by PI and robust controls under the same two resistive loads. As the results indicated, the current tracking characteristics are improved. The measured steady-state characteristics without current robust controller are listed in Table 3.2, while the ones with robust control are listed in Table 3.3.

Table 3.2: Steady-state characteristics of the developed bridgeless boost SMR by PI control under different loads

	2000 Ω	800 Ω	400 Ω
V_{ac} (V)	110.55	110.50	110.14
I_{ac} (A)	0.2443	0.5151	0.9980
P_{ac} (W)	23.72	54.77	108.57
V_{dc} (V)	201.73	200.13	200.51
I_{dc} (A)	0.1005	0.2489	0.5000
P_{dc} (W)	20.26	49.81	100.25
PF	0.8782	0.9622	0.9877
η	85.41%	90.94%	92.34%
THD_i	45.33%	24.38%	13.27%

Table 3.3: Steady-state characteristics of the developed bridgeless boost SMR by PI and robust controls under different loads

	2000 Ω	800 Ω	400 Ω
V_{ac} (V)	110.28	110.25	110.18
I_{ac} (A)	0.2369	0.5079	1.0007
P_{ac} (W)	24.26	55.00	109.53
V_{dc} (V)	203.85	202.20	201.83
I_{dc} (A)	0.1117	0.2580	0.5147
P_{dc} (W)	22.74	52.15	103.87
PF	0.9285	0.9822	0.9934
η	93.73%	94.83%	94.84%
THD_i	23.62%	11.15%	8.99%

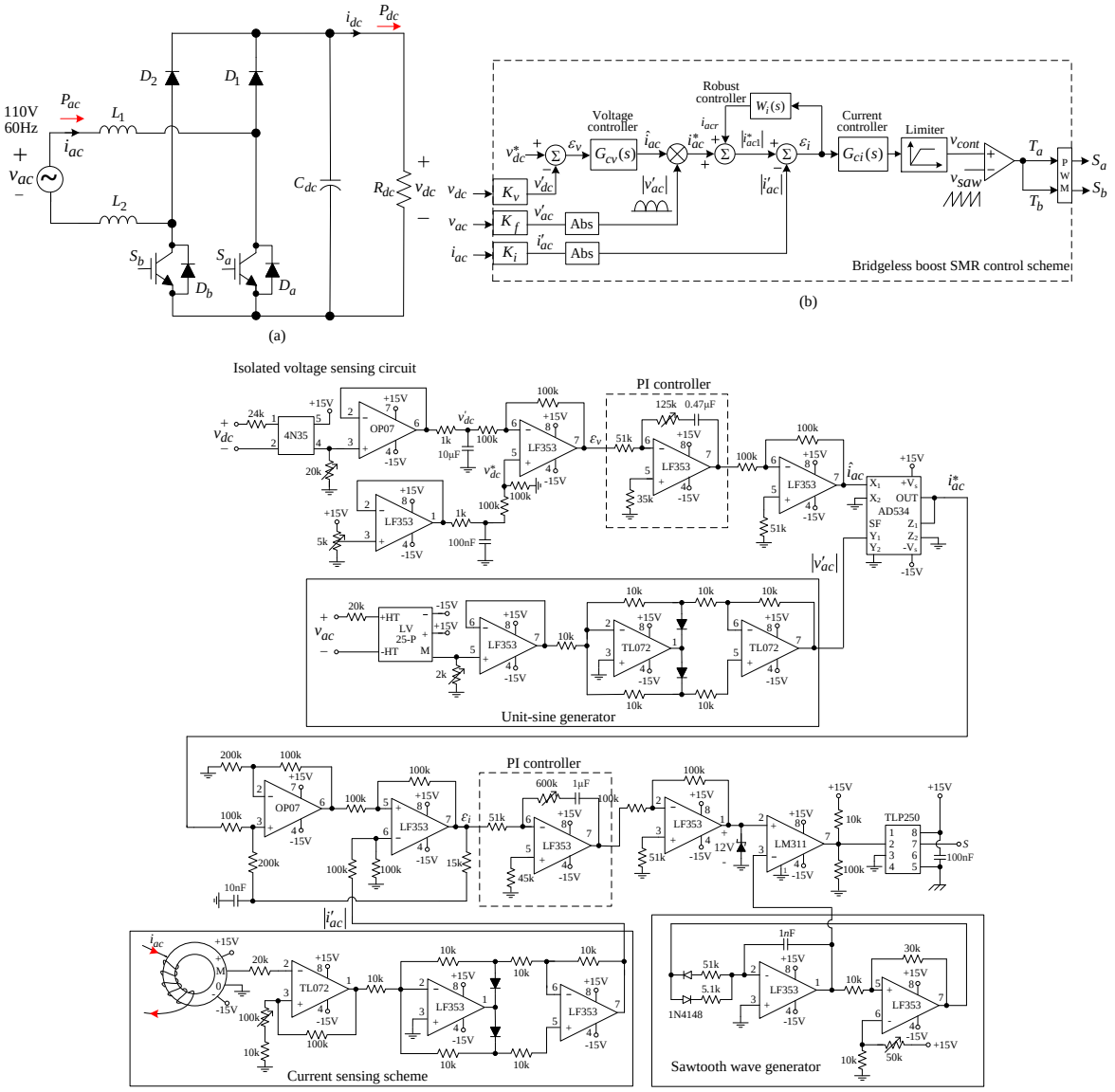

Fig. 3.3. The developed bridgeless boost SMR: (a) power circuit; (b) control scheme; (c) analog realization circuit.

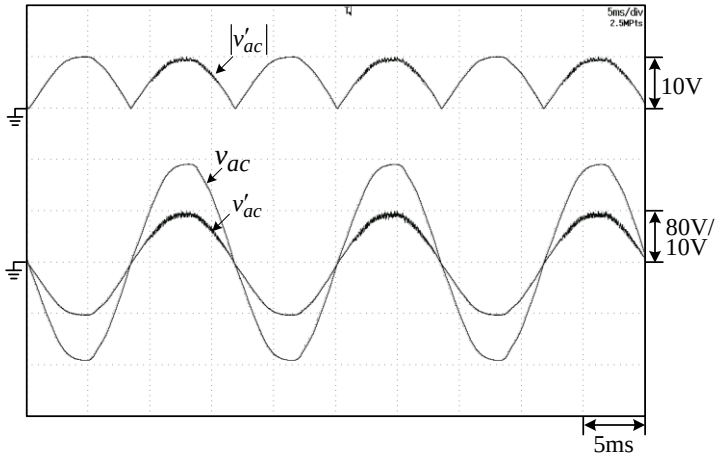

Fig. 3.4. Measured grid voltage v_{ac}, sensed voltage v'_{ac} and generated unit-sine $|v'_{ac}|$.

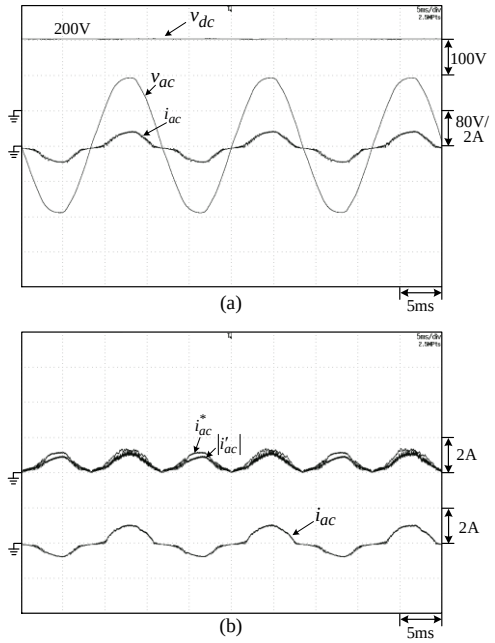

Fig. 3.5. Measured results of the established bridgeless boost SMR by PI control only at $(V_{ac} = 110\text{V}/60\text{Hz}, V_{dc} = 200\text{V}, R_{dc} = 800\Omega)$: (a) (v_{ac}, i_{ac}, v_{dc}); (b) $(i_{ac}^*, |i'_{ac}|, i'_{ac})$.

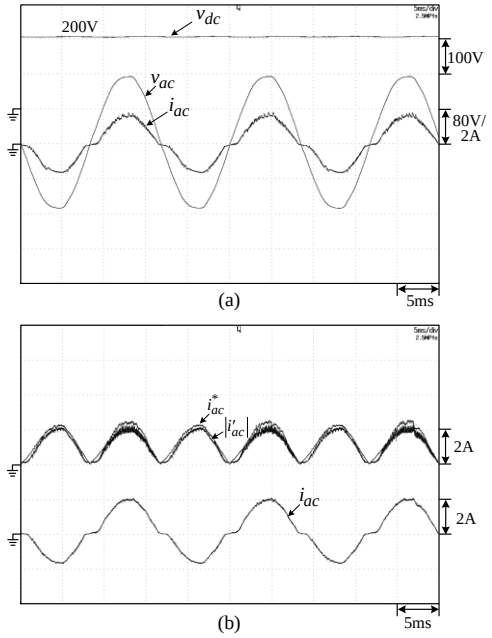

Fig. 3.6. Measured results of the established bridgeless boost SMR by PI control only at $(V_{ac} = 110\text{V}/60\text{Hz}, V_{dc} = 200\text{V}, R_{dc} = 400\Omega)$: (a) (v_{ac}, i_{ac}, v_{dc}); (b) $(i_{ac}^*, |i'_{ac}|, i'_{ac})$.

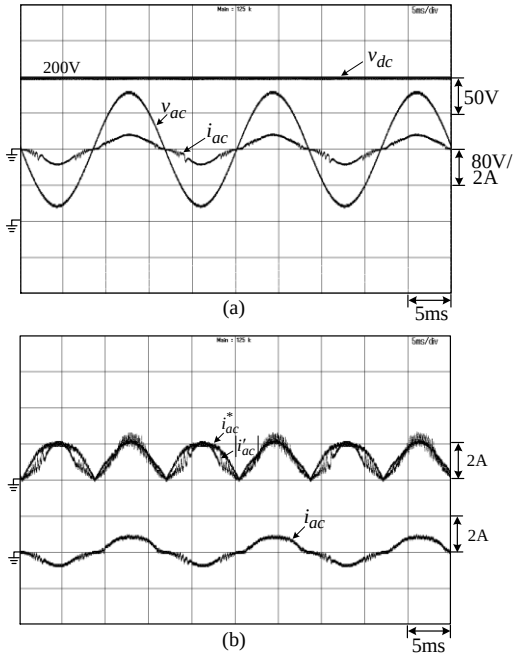

Fig. 3.7. Measured results of the established bridgeless boost SMR by PI and robust current controls at $(V_{ac} = 110\text{V}/60\text{Hz}, V_{dc} = 200\text{V}, R_{dc} = 800\Omega)$: (a) (v_{ac}, i_{ac}, V_{dc}); (b) $(i_{ac}^*, |i'_{ac}|, i'_{ac})$.

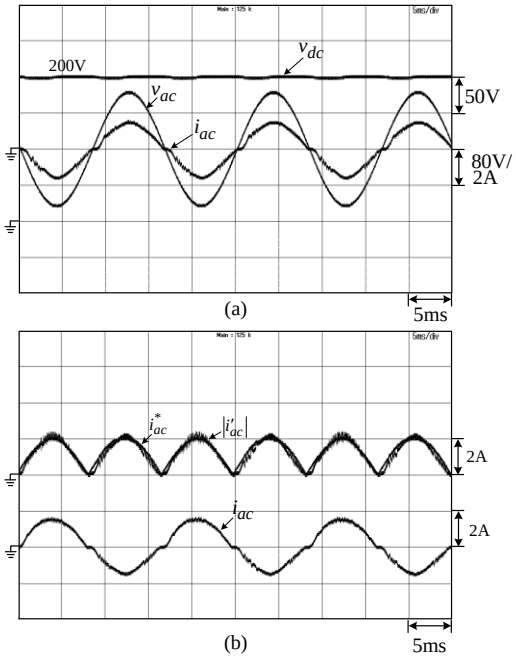

Fig. 3.8. Measured results of the established bridgeless boost SMR by PI and robust current controls at $(V_{ac} = 110\text{V}/60\text{Hz}, V_{dc} = 200\text{V}, R_{dc} = 400\Omega)$: (a) (v_{ac}, i_{ac}, V_{dc}); (b) $(i_{ac}^*, |i'_{ac}|, i'_{ac})$.

3.4. Bridgeless Boost Switch-mode Rectifier Powered Switched-Reluctance Motor Driven Cooling Fan

The power circuit of the bridgeless boost SMR powered SRM-driven fan and its control scheme are shown in Fig. 3.9. The designed controllers are listed in (1) and (2). Fig. 3.10 shows the measured results of the developed bridgeless boost SMR under different driven

speeds. The power quality of the SMR is better as the load increases. As to the SRM drive, Fig. 3.12 shows the measured SRM winding currents at three specific speeds. Normal motor operation can be seen. Finally, the measured steady-state characteristics under different driven speeds are listed in Table 3.4.

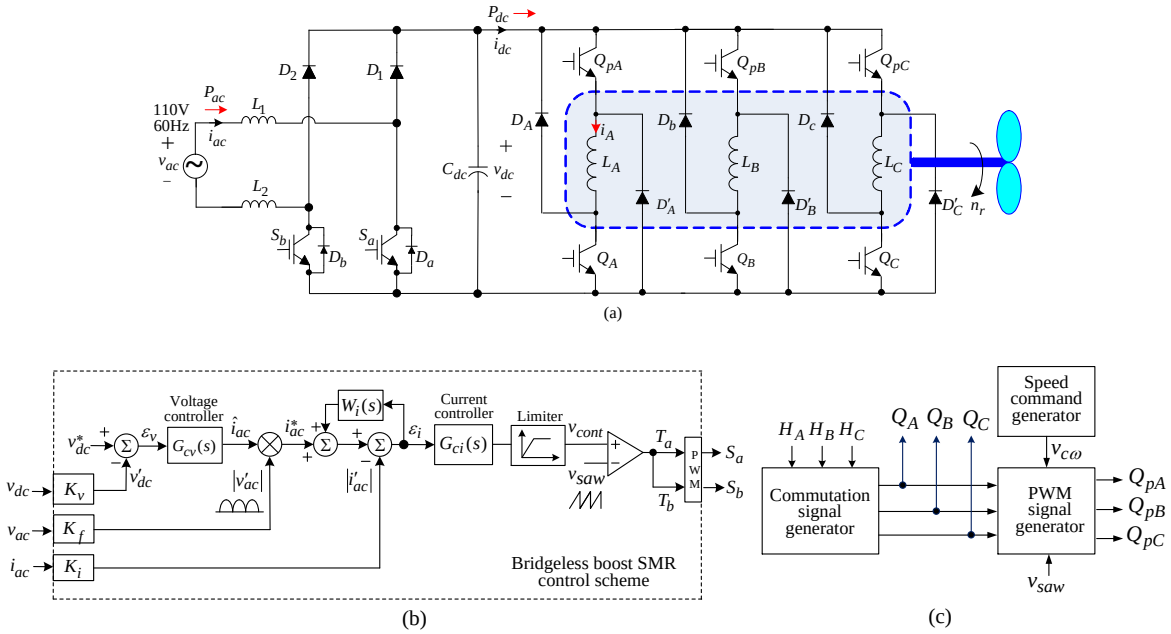

Fig. 3.9. The established bridgeless boost SMR powered switched-reluctance motor driven cooling fan: (a) power circuit; (b) SMR control scheme.; (c) SRM control scheme.

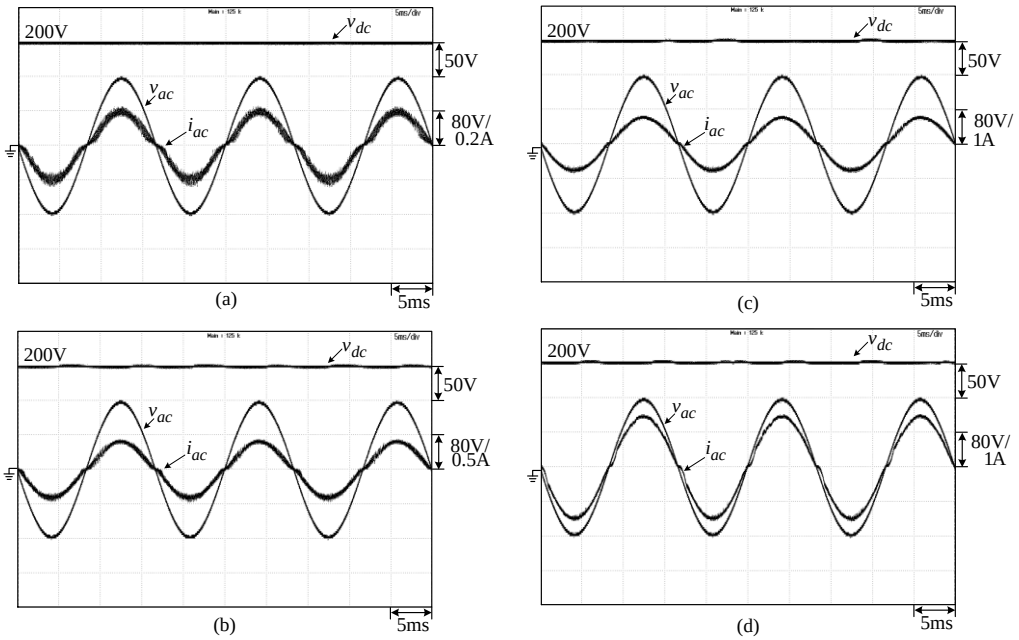

Fig. 3.10. Measured (v_{ac}, i_{ac}, v_{dc}) of the established bridgeless boost SMR under different driven speeds at $(V_{ac} = 110\text{V}/60\text{Hz}, V_{dc} = 200\text{V})$: (a) 400rpm; (b) 600rpm; (c) 800rpm; (d) 1000rpm.

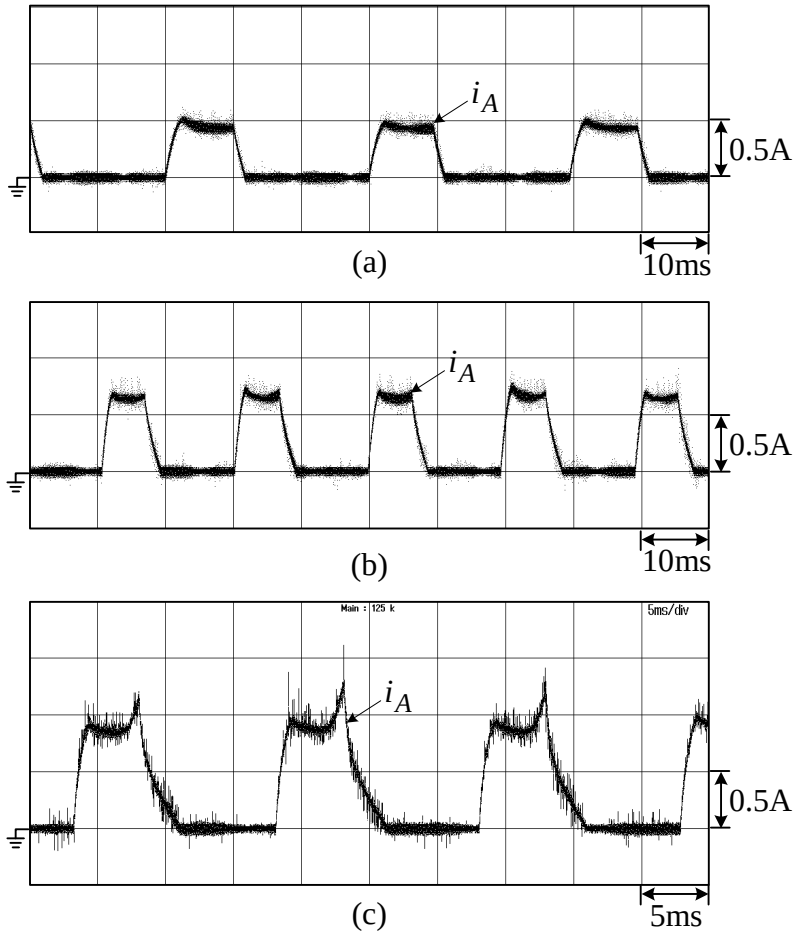

Fig. 3.11. Measured SRM winding currents under three speeds at ($V_{ac} = 110\text{V}/60\text{Hz}$, $V_{dc} = 200\text{V}$): (a) 500rpm; (b) 750rpm; (c) 1000rpm.

Table 3.4: Steady-state characteristics of bridgeless boost SMR fed SRM driven cooling fan under different speeds

	300rpm	400rpm	500rpm	600rpm	700rpm	800rpm	900rpm	1000rpm
V_{ac} (V)	110.31	110.29	110.24	110.22	110.16	110.15	110.09	109.98
I_{ac} (A)	0.1067	0.1174	0.1660	0.1978	0.2869	0.3811	0.5006	0.6651
P_{ac} (W)	9.56	10.99	16.56	20.40	30.43	40.96	54.21	72.39
V_{dc} (V)	200.43	196.69	200.96	196.51	198.45	197.23	197.75	197.23
I_{dc} (A)	0.0335	0.0442	0.0699	0.0892	0.1387	0.1925	0.2520	0.3505
P_{dc} (W)	6.70	8.69	14.03	17.52	27.52	37.96	49.75	69.11
PF	0.9000	0.9546	0.9773	0.9861	0.9921	0.9950	0.9967	0.9977
η	73.04%	79.08%	84.77%	85.92%	90.44%	92.69%	93.52%	95.47%
THD_i	12.35%	9.97%	7.66%	6.39%	5.03%	4.52%	4.51%	4.60%

3.5. Standard Boost Switch-mode Rectifier Powered Switched-Reluctance Motor Driven Cooling Fan

A. Power Circuit

The power circuit of the developed standard boost SMR powered SRM driven cooling fan is shown in Fig. 3.12(a). The system variables are listed below:

- AC input: $V_{ac} = 110\text{V}/60\text{Hz}$.
- DC output: $V_{dc} = 200\text{V}$.
- Switching frequency: $f_s = 20\text{kHz}$.
- Energy storage inductors and filtering capacitor: $L_{ac} = 7\text{mH}, C_{dc} = 1000\mu\text{F}$.
- Power switches S_{ac}: W20NK50Z

B. Control Scheme

The control scheme of the developed standard boost SMR is shown in Fig. 3.12(b). Notice that the unit-sine generation circuit is the same as Fig. 3.3. The adopted sensing factors and controller parameters are listed as followes:

$$K_v = 0.0025\text{V/V}, \quad K_f = 0.0909\text{V/V}, \quad K_i = 1.6\text{V/A} \tag{3}$$

$$G_{cv} = 2.45 + \frac{19.6}{s}, \quad G_{ci} = 11.76 + \frac{19.6}{s}, \quad W_i(s) = \frac{0.5}{1 + 0.0001s} \tag{4}$$

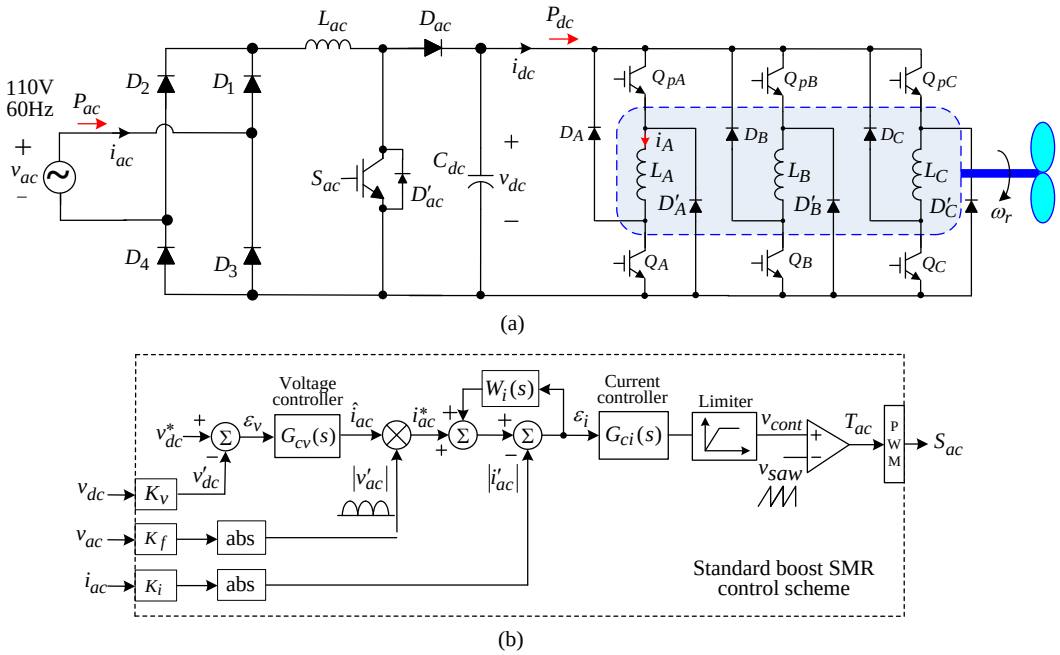

Fig. 3.12. The established standard boost SMR powered switched-reluctance motor driven cooling fan: (a) power circuit; (b) SMR control scheme.

C. Measured Results

(a) Unit-sine function

Fig. 3.13 shows the measured grid voltage v_{ac}, sensed voltage v'_{ac} and the generated unit-sine function $|v'_{ac}|$. The results indicate the successful generation of in-phase unit-sine function.

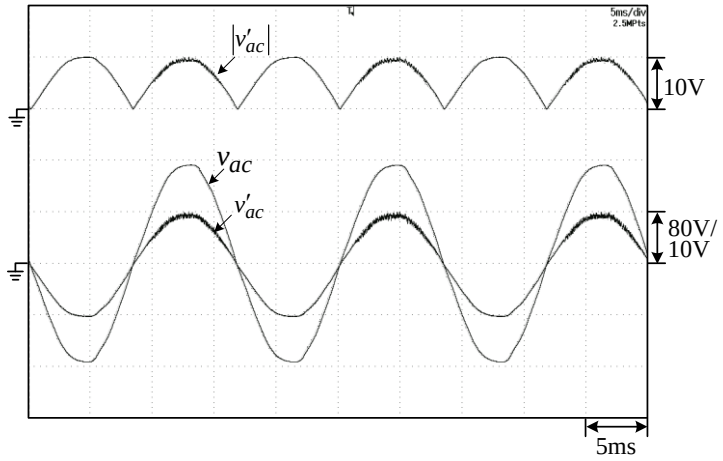

Fig. 3.13. Measured grid voltage v_{ac}, sensed voltage v'_{ac} and generated unit-sine $|v'_{ac}|$.

(b) Steady-state characteristics

Fig. 3.14 shows the measured results of the developed standard boost SMR under two resistive loads. And the measured steady-state characteristics under three loads are listed in Table 3.5.

Table 3.5: Steady-state characteristics of the established standard boost SMR under three resistive loads

	2000 Ω	800 Ω	400 Ω
V_{ac} (V)	110.09	110.06	110.09
I_{ac} (A)	0.2117	0.4867	0.9731
P_{ac} (W)	22.79	53.19	106.83
V_{dc} (V)	200.65	201.18	199.97
I_{dc} (A)	0.1090	0.2583	0.5275
P_{dc} (W)	21.88	51.97	105.48
PF	0.9781	0.9930	0.9972
η	96.00%	97.70%	98.74%
THD_i	5.72%	5.08%	4.70%

Fig. 3.15 plots the measured results of the established standard boost SMR powered SRM-driven fan under different driven speeds. The measured steady-state characteristics are listed in Table 3.6. The comparative efficiencies and power factors of the bridgeless and standard boost SMR powered SRM cooling fans listed in Tables 3.4 and 3.6 are plotted in Fig. 3.16.

In addition, Fig. 3.17 plots the comparative efficiencies and power factors of the diode rectifier, the bridgeless boost SMR and the standard boost SMR powered SRM cooling fans listed in Tables 3.1, 3.4 and 3.6. Since the diode rectifier fed cooling fan can not be operated over 700rpm due to lacking of DC output voltage regulation ability, only the results below 700rpm are presented. It is obviously that: (i) the diode rectifier possesses the highest efficiency subject to having bad power quality characteristics. Moreover, the driven speed range is relatively narrow; (ii) the bridgeless boost SMR possesses the higher efficiencies and better power factors compared to standard boost SMR.

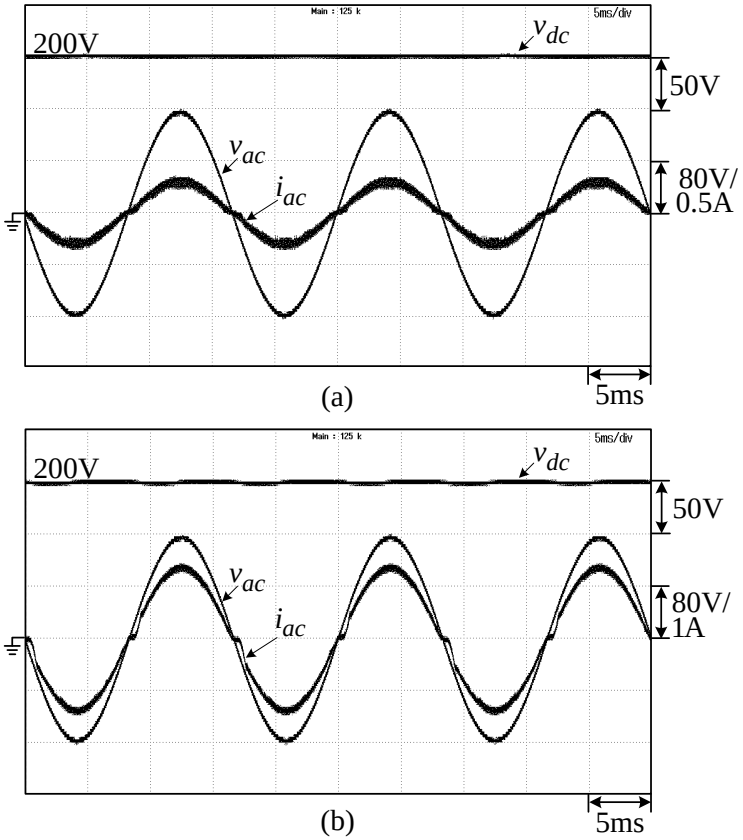

Fig. 3.14. Measured (v_{ac}, i_{ac}, v_{dc}) of the established standard boost SMR under two resistive loads at $(V_{ac} = 110\text{V}/\ 60\text{Hz}, V_{dc} = 200\text{V})$: (a) $R_{dc} = 2000\Omega$; (b) $R_{dc} = 400\Omega$.

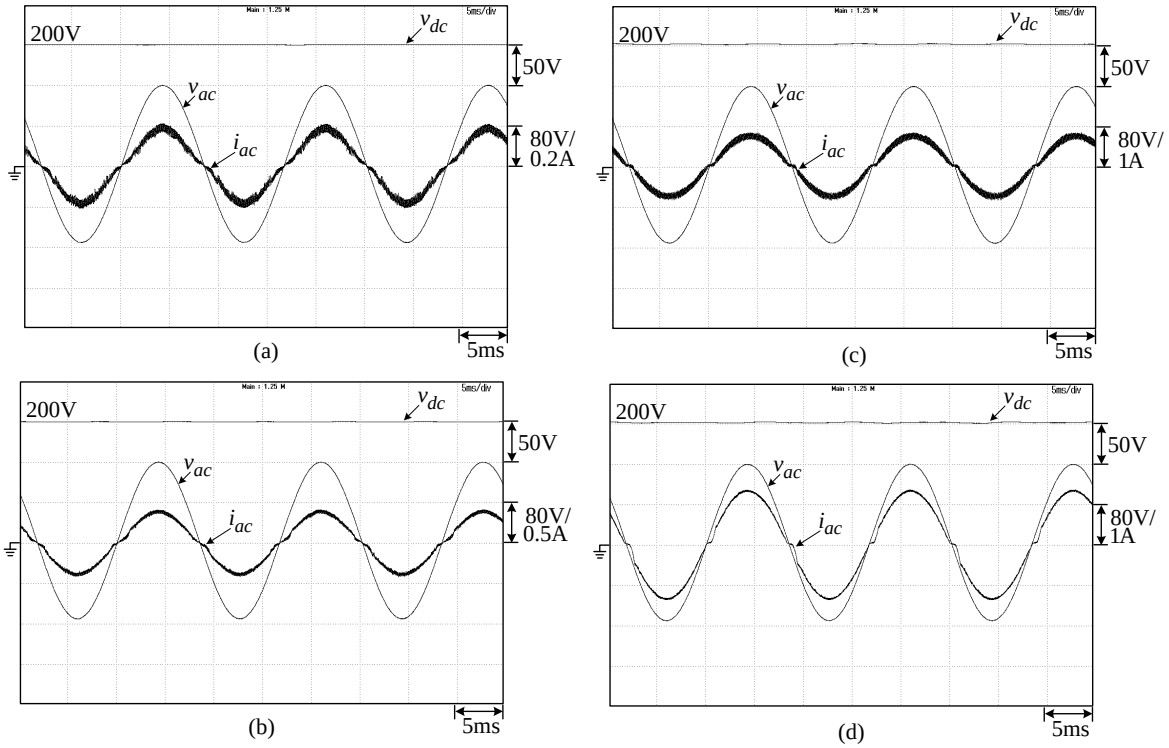

Fig. 3.15. Measured (v_{ac}, i_{ac}, v_{dc}) results of the established standard boost SMR powered SRM-driven fan under different speeds at $(V_{ac} = 110\text{V}/60\text{Hz}, V_{dc} = 200\text{V})$: (a) 400rpm; (b) 600rpm; (c) 800rpm; (d) 1000rpm.

Table 3.6: Steady-state characteristics of standard boost SMR fed SRM driven cooling fan under different speeds

	300rpm	400rpm	500rpm	600rpm	700rpm	800rpm	900rpm	1000rpm
V_{ac} (V)	110.32	110.32	110.32	110.31	110.31	110.30	110.30	110.28
I_{ac} (A)	0.0877	0.1037	0.1403	0.1985	0.2681	0.3628	0.4800	0.6233
P_{ac} (W)	8.43	10.45	14.71	21.33	29.12	39.65	52.66	68.51
V_{dc} (V)	201.14	201.03	200.83	200.69	200.64	200.66	200.93	200.53
I_{dc} (A)	0.0304	0.0403	0.0607	0.0899	0.1292	0.1814	0.2439	0.3215
P_{dc} (W)	6.11	8.10	12.19	18.04	25.92	36.40	49.01	64.47
PF	0.8720	0.9138	0.9507	0.9742	0.9847	0.9908	0.9946	0.9965
η	72.51%	77.51%	82.80%	84.65%	88.95%	91.79%	93.06%	94.10%
THD_i	13.83%	11.80%	10.21%	8.15%	6.96%	6.06%	4.61%	4.00%

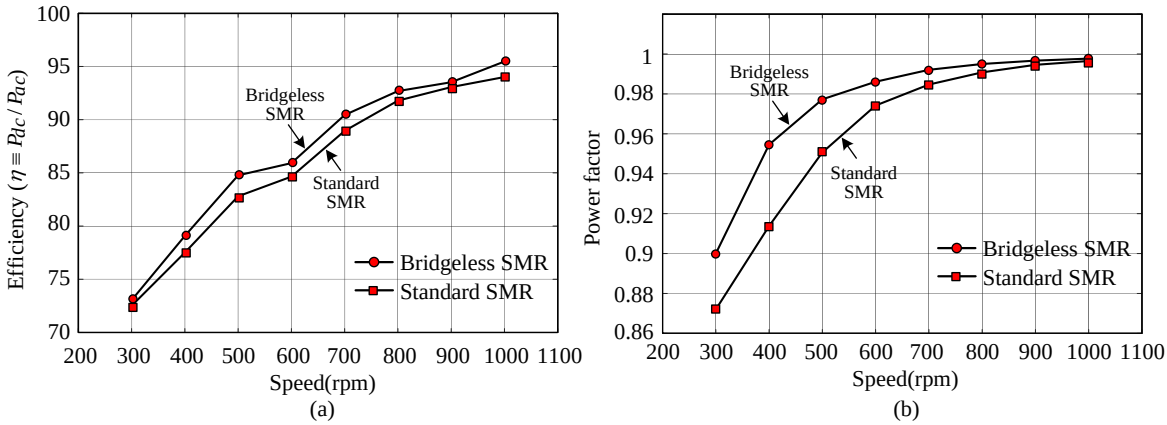

Fig. 3.16. Comparative efficiencies and power factors of the bridgeless and standard boost SMRs powered SRM cooling fans listed in Tables 3.4 and 3.6.

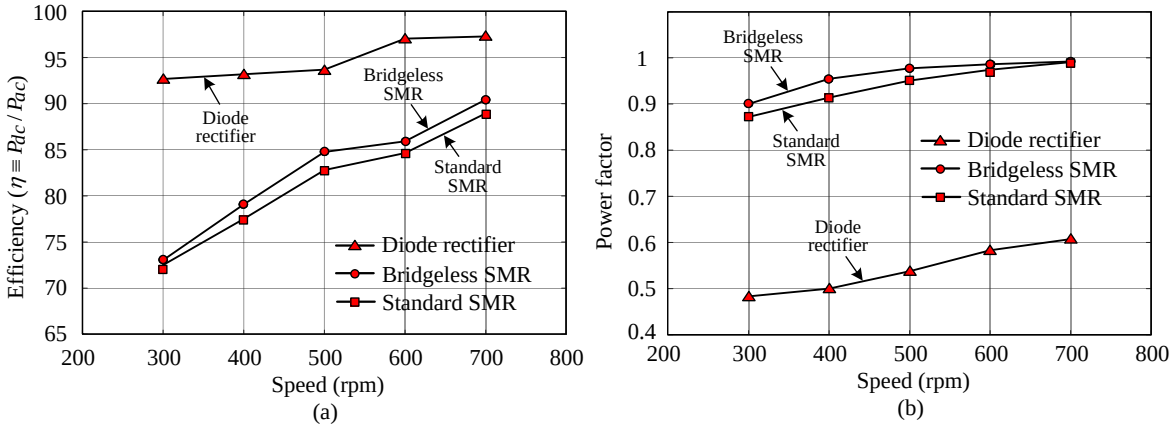

Fig. 3.17. Comparative efficiencies and power factors of diode rectifier, bridgeless boost SMR and standard boost SMR powered SRM cooling fans.

IV. CONCLUSIONS

This special topic has presented the development of a bridgeless boost SMR powered SRM driven cooling fan. The power circuit and control scheme are all properly designed. Thanks to the bridgeless schematic, it possesses higher efficiency compared with the standard SMR.

The comparative performance evaluation for the cooling fan powered by the diode rectifier, the standard boost SMR and the bridgeless boost SMR is made in details. Some comments can be concluded for the results: (i) the diode rectifier possesses the highest efficiency subject to having bad power quality characteristics. Moreover, since diode rectifier lacks of output DC voltage regulating ability, cooling fan can not be operated over 700rpm; (ii) the bridgeless boost SMR possesses the higher efficiencies and better power factors compared to standard boost SMR.

REFERENCES

[1] N. Mohan, T. M. Undeland, and W. P. Robbims, *Power Electronics: Converters, Applications and Design*, 1995, New York: John Wiley & Sons.

[2] T. J. E. Miller, *Switched Reluctance Motors and Their Control*, Clarendon Press, Oxford, 1993.

[3] E. Bostanci, M. Moallem, A. Parsapour, and B. Fahimi, "Opportunities and challenges of switched reluctance motor drives for electric propulsion: a comparative study," *IEEE Trans. Transport. Electrific*., vol. 3, no. 1, pp. 58-75, Mar. 2017.

[4] J. O. Fiedler and R. W. De Doncker, "Designing low-cost switched reluctance drives for fan-applications," in *Proc. IEEE PEMD*, 2002, vol. 2, pp. 758-762.

[5] M. Cacciato, A. Consoli, G. Scarcella, and G. Scelba, "A switched reluctance motor drive for home appliances with high power factor capability," in *Proc. IEEE PESC*, 2008, pp. 1235-1241.

[6] Y. W. Lin, K. F. Chou, M. J. Yeh, C. C. Wang, S. L. Yu, C. C. Yang, Y. C. Chang, and C. M. Liaw, "Design and control of a switched-reluctance motor-driven cooling fan," *IET Power Electron.*, vol. 5, no. 9, pp. 1813-1826, 2012.

[7] S. M. Castano, J. Maixe-Altes, and A. Emadi, "Development and performance analysis of a switched reluctance motor drive for an automotive air-conditioning system," in *Proc. IEEE ITEC*, 2016.

[8] S. Vukosavic and V. R. Stefanovic, "SRM inverter topologies: a comparative evaluation," *IEEE Trans. Ind. Appl*., vol. 27, no. 6, pp. 1034-1049, 1991.

[9] M. Barnes and C. Pollock, "Power electronic converters for switched reluctance drives," *IEEE Trans. Power Electron*., vol. 13, no. 6, pp. 1100-1111, 1998.

[10] V. V. Deshpande and Y. L. Jun, "New converter configurations for switched reluctance motors wherein some windings operate on recovered energy," *IEEE Trans. Ind. Appl.*, vol. 38, no. 6, pp. 1558-1565, 2002.

[11] H. C. Chang and C. M. Liaw, "An integrated driving/charging switched reluctance motor drive using three-phase power module," *IEEE Trans. Ind. Electron.*, vol. 58, no. 5, pp. 1763-1775, 2011.

[12] F. Peng, J. Ye, and A. Emadi, "An asymmetric three-level neutral point diode clamped converter for switched reluctance motor drives," *IEEE Trans. Power Electron*., vol. 32, no. 11, Nov. 2017.

[13] FCAS20DN60BB smart power module for SRM, www.fairchildsemi.com/ds/ FC/FCAS20DN60BB.pdf.

[14] N. Mohan, T. M. Undeland, and W. P. Robbims, *Power Electronics: Converters, Applications and Design*, 1995, New York: John Wiley & Sons.

[15] W. Huai and I. Batarseh, "Comparison of basic converter topologies for power factor correction," in *Proc. IEEE SECON*, 1998, pp. 348-353.

[16] O. Garcia, J. A. Cobos, R. Prieto, P. Alou, and J. Uceda, "Single phase power factor correction: a survey," *IEEE Trans. Power Electron.*, vol. 18, no. 3, pp.749-755, 2003.

[17] B. Singh, B. N. Singh, A. Chandra, K. Al-Haddad, A. Pandey, and D. P. Kothari, "A review of single-phase improved power quality AC-DC converters," *IEEE Trans. Ind. Electron*., vol. 50, no. 5, pp. 962-981, 2003.

[18] L. Huber, J. Yungtaek, and M. M. Jovanovic, "Performance evaluation of bridgeless PFC boost rectifiers," *IEEE Trans. Power Electron*., vol. 23, no. 3, pp. 1381-1390, 2008.

[19] G. Moschopoulos and P. Jain, "Single-phase single-stage power-factor-corrected converter topologies," *IEEE Trans. Ind. Electron.*, vol. 52, no. 1, pp. 23-35, 2005.

[20] Y. T. Jang and M. M. Jovanović, "A bridgeless PFC boost rectifier with optimized magnetic utilization," *IEEE Trans. Power Electron.*, vol. 24, no. 1, pp. 85-93, Jan. 2009.

[21] F. Musavi, W. Eberle, and W. G. Dunford, "A high-performance single-phase bridgeless interleaved PFC converter for plug-in hybrid electric vehicle battery chargers," *IEEE Trans. Ind. Appl*., vol. 47, no. 4, pp. 1833-1843, Jul./ Aug. 2011.

[22] F. Musavi, M. Edington, W. Eberle, and W. G. Dunford, "Evaluation and efficiency comparison of front end AC-DC plug-in hybrid charger topologies," *IEEE Trans. Smart Grid*, vol. 3, no. 1, pp. 413-421, Mar. 2012.

Appendix: Photos of the established SRM driven cooling fan

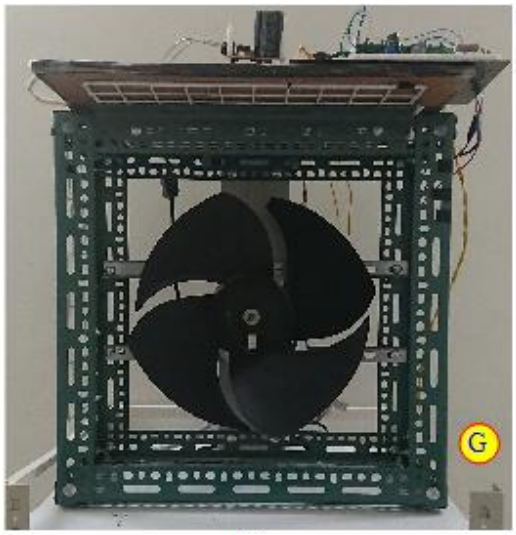

(a)

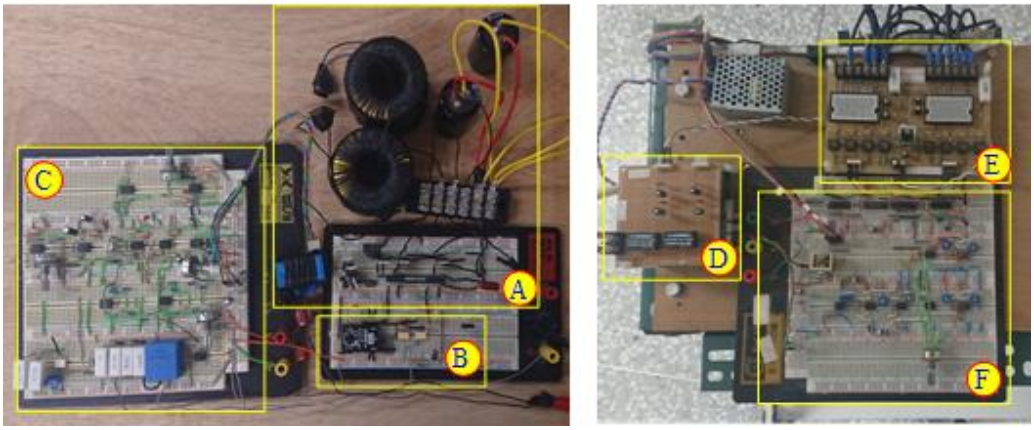

Ⓐ Bridgeless boost SMR
Ⓑ Gate driver of boost SMR
Ⓒ Analog control circuit of boost SMR
Ⓓ Power supply module
Ⓔ SRM asymmetric bridge converter
Ⓕ Analog control circuit of SRM drive
Ⓖ SRM driven fan

(b)